

## **Pattern Formation Dynamics in Diverse Physico-Chemical Systems**

**Tony Karam, Houssam El-Rassy, Victor Nasreddine, Farah Zaknoun,  
Samia El-Joubaily, Amal Zein Eddin, Hiba Farah, Jad Husami,  
Samih Isber† and Rabih Sultan\***

Departments of Chemistry and †Physics, American University of Beirut, Beirut,  
Lebanon  
E-mail: rsultan@aub.edu.lb

**Abstract:** Complex reaction-transport dynamics can lead to the formation of ordered structures. A constant dissipation of free energy is a requirement for sustaining macroscopic order, especially in solution. In the solid phase, the evolved pattern can be locked for days, months or even years. Liesegang bands are stratified stripes of precipitate that appear and persist, when co-precipitate ions interdiffuse in a gel medium. A host of interesting properties characterize such rich dynamical systems: band spacing laws (direct and revert), band splitting, rhythmic multiplicity, multiple precipitate formation and band redissolution are but a few manifested characteristics, emerging from a complex dynamics with a great diversity of scenarios.

The familiar and well-known band formation in rocks could be the result of a complex coupled diffusion-percolation-chemical reaction mechanism. Similarities between geochemical self-organization and the Liesegang phenomenon are surveyed and analyzed. The simulation of band generation in a rock bed is realized and carried out in-situ, by injection and infusion of the reactant components into the rock medium.

Ramified, tree-like structures (dendrites) are obtained during the electrodeposition or simple electroless redox deposition of metal systems. A great variety of morphologies just resembling tree branches are observed and characterized as fractal structures.

**Keywords:** Liesegang, dendrites, reaction-diffusion, rock banding.

### **1. Liesegang Banding**

In 1896, Raphael Eduard Liesegang discovered an intriguing phenomenon [1] whereby precipitation in a gel medium takes place in banded form, just like the superb display of bands that we commonly observe in rocks [2-4]. Various specimens of Liesegang patterns, prepared for different precipitates, are shown in Fig. 1.



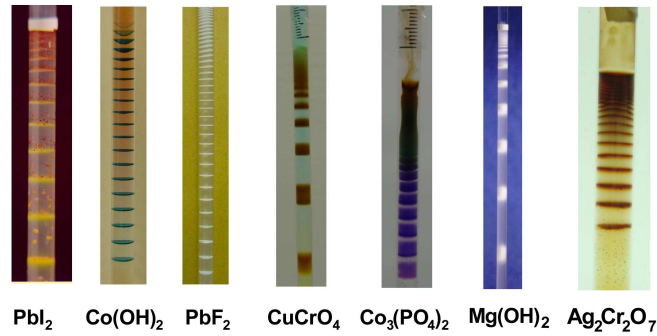


Figure 1: A panorama of colorful Liesegang patterns in gel.

In the laboratory, the Liesegang experiment [5-7] is quite simple: a concentrated electrolyte containing a certain co-precipitate ion (say  $\text{Pb}^{2+}$ ) is allowed to diffuse into a gel containing its insoluble salt counterpart (such as  $\text{I}^-$  to form  $\text{PbI}_2$ ); normally one order of magnitude more dilute. Due to the coupling of diffusion to a cycle of supersaturation, nucleation and depletion, known as the Ostwald cycle [8], the precipitation takes place in the form of beautifully stratified bands, as displayed in Fig. 1.

We highlight the main features of such a rich dynamical phenomenon, but also shed light on abnormalities, curiosities and strange behavior exhibited by such systems under certain conditions. The observations common to most Liesegang systems are summarized by the four well-known empirical laws [9,10]:

<p><i>Time law:</i> <math>x_n = \sqrt{at_n}</math></p>	<p><i>Spacing law:</i> <math>\rho_n = \frac{x_{n+1}}{x_n} \rightarrow 1+p</math> as as <math>n</math> is large.</p>
<p><i>Width law:</i> <math>w_n = mx_n^\alpha \quad \alpha &gt; 0</math></p>	<p><i>Matalon-Packter law:</i> <math>p = F(b_0) + \frac{G(b_0)}{a_0}; \begin{cases} a_0 \text{ conc. of outer} \\ b_0 \text{ conc. of inner} \end{cases}</math></p>

where  $n$  denotes band number,  $x$  is location and  $w$  is band width. The spacing law formula suggests that the spacing between consecutive bands increases as we move away from the electrolytes junction. Although 90% of the Liesegang patterns follow this so-called Jablczynski spacing law [11], some systems exhibit an opposite trend, known as *revert* spacing [12,13]. The distinction between *direct* and *revert* spacing Liesegang patterns is depicted in Fig. 2.

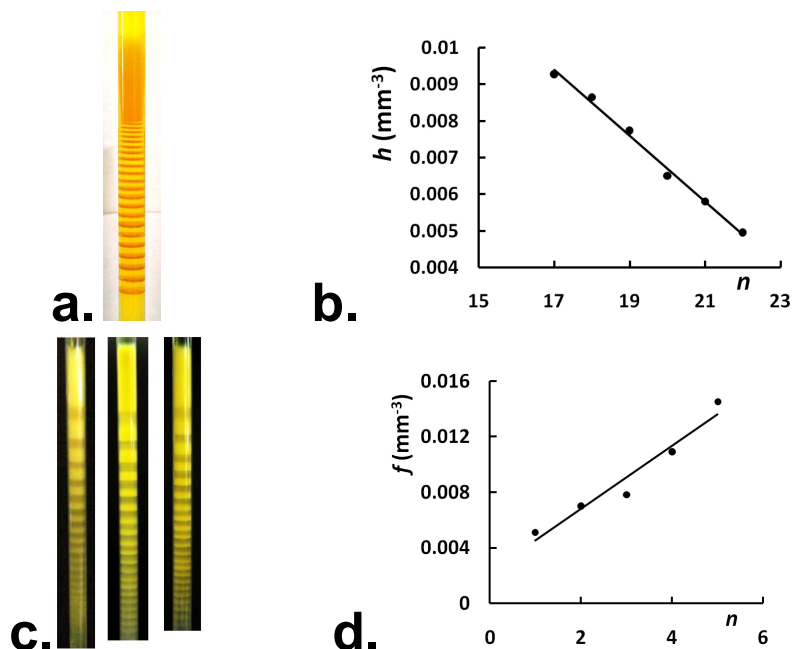


Figure 2: a. Liesegang pattern of  $\text{CuCrO}_4$  showing direct (normal) spacing. b. Plot of fraction of adsorbed  $\text{CrO}_4^{2-}$  on the copper chromate precipitate ( $h$ ) with band number. c. Liesegang patterns of  $\text{PbCrO}_4$  showing *revert* spacing. d. Plot of fraction of adsorbed  $\text{CrO}_4^{2-}$  on the lead chromate precipitate ( $f$ ) with band number. We see that  $h$  decreases while  $f$  increases.

In a recent study [13], we showed that the fraction of  $\text{CrO}_4^{2-}$  adsorbed ( $f$ ) on the lead chromate precipitate increases with band number  $n$  (see Fig. 2d); whereas the opposite trend was observed for the adsorption on copper chromate (the fraction  $h$  decreases with band number  $n$ ; as seen in Fig. 2b). Hence the increased extent of adsorption causes the bands to form closer and closer as  $n$  increases. It seems that more  $\text{CrO}_4^{2-}$  adsorbed attract the  $\text{Pb}^{2+}$  in the gel closer than in the preceding band, thus causing the precipitate band to form closer, and the spacing to become narrower. The opposite behavior (decreasing extent of adsorption with band number as in Fig. 2b) results in a normal Liesegang pattern with direct spacing (Figure 2a).

Liesegang systems exhibit a great diversity of special features. A pattern of bands seemingly 'migrates' if redissolution of the bands at the top is synchronized with the band formation. Such scenario occurs in systems where the precipitate redissolves to form a complex ion. Typical studied examples include the  $\text{Co}(\text{OH})_2$  [14,15],  $\text{Cr}(\text{OH})_3$  [16] and  $\text{HgI}_2$  [17] systems. When  $\text{Co}(\text{OH})_2$  is precipitated from  $\text{Co}^{2+}$  and  $\text{NH}_4\text{OH}$ , the precipitate redissolves in excess  $\text{NH}_4\text{OH}$  to form the hexaammine cobalt (II) complex ion,  $\text{Co}(\text{NH}_3)_6^{2+}$ , according to the reaction:

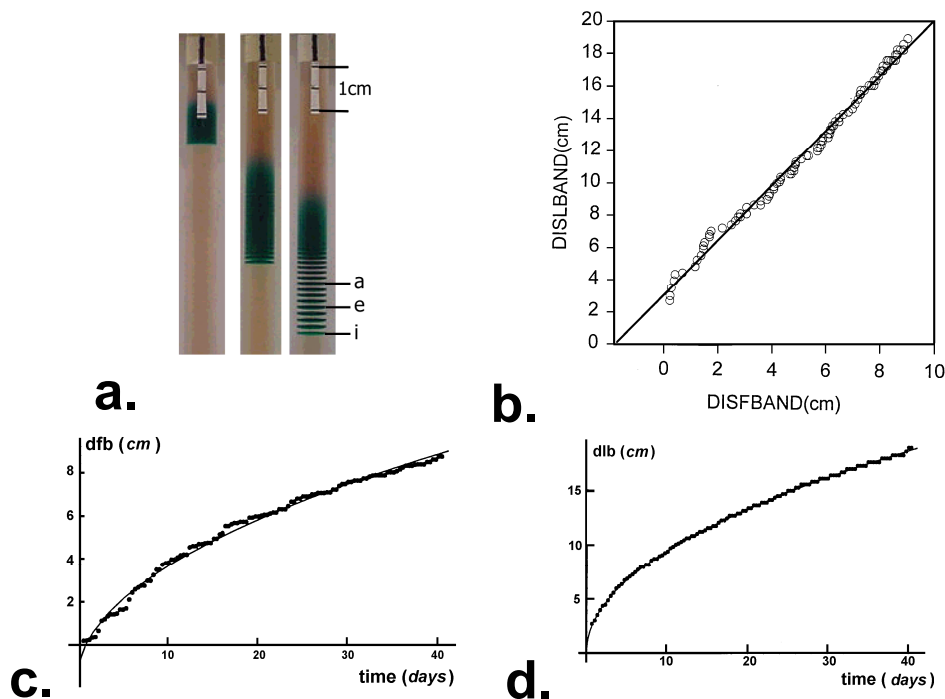
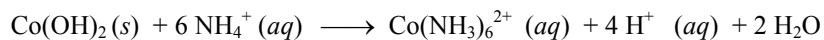


Figure 3: a. Propagating  $\text{Co(OH)}_2$  Liesegang pattern via a concerted band formation and band redissolution scenario. b. Correlation plot showing the linear correlation between the distance of last band ( $dlb$ ) and distance of first band ( $dfb$ ). c. Plot of  $dfb$  versus time. d. Plot of  $dlb$  versus time. The two parameters are controlled by diffusion.

The precipitation-redissolution-propagation of the  $\text{Co(OH)}_2$  pattern of bands is illustrated in Fig. 3a. The distance of the top edge of the propagation zone ( $dfb$ ) and the distance of the last band ( $dlb$ ) are plotted versus time in days. The plots are shown in Figs. 3c and 3d. We see that the propagation at the top and the bottom is dominated by diffusion. The correlation between  $dfb$  and  $dlb$  is almost perfectly linear [14], as revealed by the correlation plot in Fig. 3b.

A host of other diverse features are observed in Liesegang systems. To name but a few, we report secondary banding [18], spiral and helicoidal patterns [19] and two-precipitate dynamics [20].

## 2. Geochemical Banding

Perhaps the most common and most spread resemblance between Liesegang patterns and natural phenomena is the landscape of bands that we observe in rocks [21,2,3]. Many studies have emphasized such similarity, presented

coherent explanations and proposed mechanisms. Theoretical modeling studies are extensive in the literature [21]. Possible scenarios range from cyclicity in large mafic-ultramafic layered intrusions, to fractional crystallization in magmatic processes, to temperature-pressure changes in both first and second-order phase transitions, to nonlinear reaction-diffusion dynamics.

In a recent work, we attempted to simulate geochemical banding (or self-organization) in-situ, i.e. inside the rock bed [22,23].

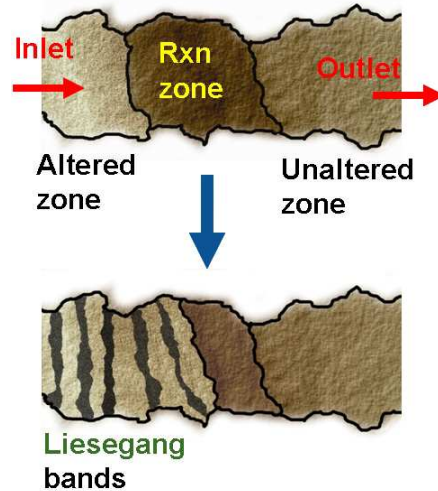
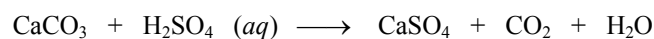


Figure 4: Liesegang bands in a rock bed behind a reaction front. The infiltrating water carries a co-precipitate ion that meets its counter ion in the rock medium and thus precipitation takes place; but it does so but in banded form, just resembling a Liesegang pattern.

Consider a porous rock infiltrated from one side by an inlet flow of reactive water, that causes the dissolution of certain constituent rock minerals. The water flow, acting as a sink of co-precipitate ions for the altered rock, can provoke the precipitation and deposition of other insoluble minerals. In many such situations, the minerals deposition occurs in banded form, in a way that just resembles the Liesegang bands obtained in a lab experiment. Such a plausible scenario is illustrated in Fig. 4.

In the lab, a ferruginous limestone rock with a planar surface (Figure 5) was infiltrated through a thin tube inserted at its center by a 4.30 M  $H_2SO_4$  solution by means of a multi-rate infusion pump. The acid causes the dissolution of calcite ( $CaCO_3$ ) and the precipitation of the acid-insoluble gypsum ( $CaSO_4$ ) and anhydrite ( $CaSO_4 \cdot 2H_2O$ ) according to the reaction:



Due to the spatio-temporal flow, the deposition of  $\text{CaSO}_4$  is anticipated to occur in banded form in accordance with the above described Liesegang dynamics (Sect. 1).

The experiment was kept running for about two years (692 days). The appearance of the various banded zones at  $t = 202$  days is depicted in Fig. 5a. The latter were delineated and labeled by tracing contours defining the inner and outer edges of each zone (Figure 5b at 692 days). The gypsum/anhydrite content of regions 1 through 7 of Fig. 5b was determined by powder X-ray diffraction. The results are shown in Table 1.

Table 1:  $\text{CaSO}_4$  composition over the various zones of Fig. 5

Region	1	2	3	4	5	6	7
% $\text{CaSO}_4$	100	97.5	98.9	28.4	85.8	17.6	5.4

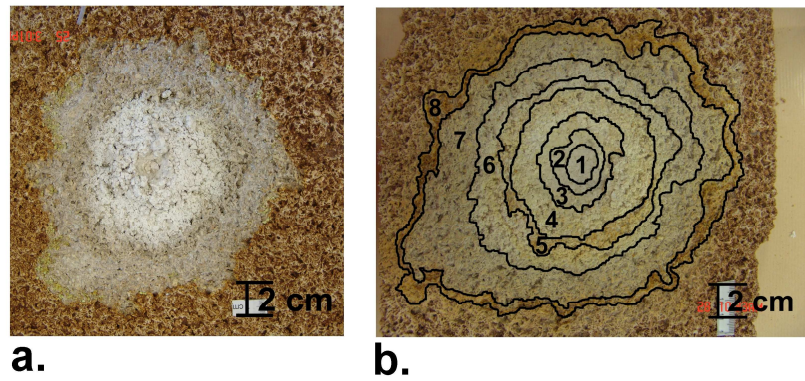
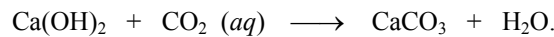


Figure 5: Acidization of a ferruginous limestone rock, by slow injection of  $\text{H}_2\text{SO}_4$  at the center causing the dissolution of calcite ( $\text{CaCO}_3$ ). The front is accompanied by the deposition of gypsum ( $\text{CaSO}_4$ ) and anhydrite ( $\text{CaSO}_4 \cdot 2\text{H}_2\text{O}$ ). a. At  $t = 202$  days. b. 'Concentric' deposition zones exhibiting oscillation in the  $\text{CaSO}_4$  content at  $t = 692$  days.

We clearly see that beyond the central region where the deposition of  $\text{CaSO}_4$  is maximal (bands 1-3), the  $\text{CaSO}_4$  content starts oscillating.

Very few other simulations of rock banding in-situ were attempted by a number of investigators. Rodriguez-Navarro et al. [24] observed Liesegang rings by monitoring the slow carbonation of traditional, aged lime mortars. A portlandite [ $\text{Ca}(\text{OH})_2$ ]/quartz mortar kept for a long time under excess,  $\text{CO}_2$ -rich water gives rise to a calcite ( $\text{CaCO}_3$ ) deposit, via the reaction:



The carbonation process yields 3D Liesegang patterns consisting of concentric ellipsoids of alternating calcite and calcite-free zones. The rings exhibit revert spacing instead of direct spacing and obey Jablczynski's spacing law. The revert

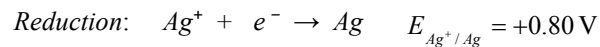
nature of the pattern was attributed to the decrease in CO<sub>2</sub> uptake and diffusion as the process progresses toward the core.

### 3. Dendritic Metal Deposits

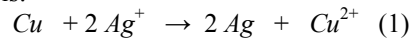
Another intriguing class of pattern formation in solid structures is the ramified, tree-like structures we observe in metal deposits [25,26]. Two routes are known for obtaining metal deposits: electrolytic and electroless. In the former, metal ions are reduced by standard electrolysis at the cathode. In the latter, a spontaneous redox reaction is carried out in the supporting medium. We perform such a study on Ag metal deposits, by growing the latter via both methods.

#### Electroless

Silver metal was deposited by reduction of Ag<sup>+</sup> with metallic copper according to the following scheme:

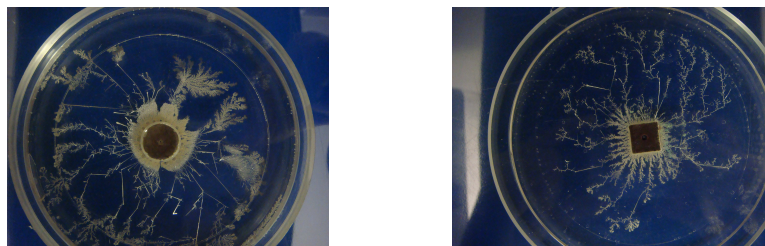


The overall reaction is:



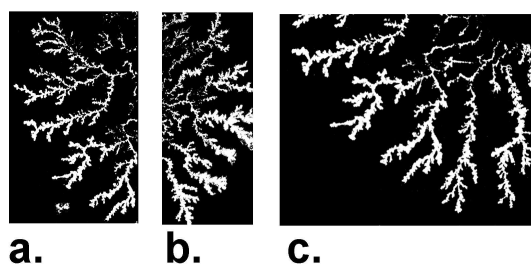
To that end, a shallow methacrylate glass (plexiglass) dish of 10.5 cm diameter was manufactured, mounted with a peripheral ring of 0.3 mm height acting as a spacer, on top of which a plexiglass cover can rest. The solution layer thickness will thus be 0.3 mm. The cover has a 1.50 cm hole, wherein a well-fitted metallic disc (here Cu) can be inserted.

With the perforated cover on, a solution of silver nitrate of known concentration (say 0.10 M), was carefully poured through the cover hole, until it spread evenly and without air bubbles throughout the dish area. Once such a thin solution film is achieved, the copper disk is placed at the center, marking the start of the spontaneous reaction (1). One important variant from other electroless growth experiments is the bare solution medium, without soaking in a filter paper to lock the pattern. After big experimental challenges, the preliminary appearance of the fractal growth (seemingly promising) is displayed in Fig. 6.



**a.** **b.**  
 Figure 6: Silver deposits showing dendritic structure growth. a. Circular disc of reductant (Cu). b. Square Cu disc.

An interesting observation is that the ramifications display straight, stringy branches in the circular core, whereas they exhibit curved branching with the square core. Different regions of the Ag deposits were cut, and the images transformed into black and white, for good contrast. Samples are depicted in Fig. 7.



**a.** **b.** **c.**  
 Figure 7: Selected regions from the deposits in Fig. 6a after transformation of the image to black and white. The three regions (a-c) essentially exhibit the same value of the fractal dimension.

The dendrites exhibited a fractal dimension of  $1.58 \pm 0.04$ .



**a.** **b.**  
 Figure 8: a. Ag deposits by electrolysis in a circular field with potential difference of 3.09 V. b. Ag deposits via reduction of  $\text{Ag}^+$  by Cu in a horizontal magnetic field of 0.50 T.

### Electrolysis

Figure 8a shows a 'rosette' obtained by electrodeposition at a graphite electrode immersed in the solution at the dish center. The anode is a circular tungsten wire electrode of 0.5 mm diameter thickness.

Figure 8b displays electroless Ag deposits from the reduction of  $\text{Ag}^+$  by metallic Cu, in the presence of a horizontal magnetic field of 0.50 T applied across the dish. The striking differences in the morphology (compare Figs 6a and 8b) reveal the importance, complexity and rich dynamics of metal deposition and growth. These observations are under continuing investigation at the present time.

Other dynamical studies of complex fractal structure in metal deposition systems include the simultaneous growth of two metals [27,28] and the effect of electric [29] and magnetic fields [30,31] in electroless and electrolytic systems.

**Acknowledgements:** This work was supported by the University Research Board (URB) of the American University of Beirut (AUB); and the Lebanese National Council for Scientific Research (LNCSR).

### References

1. R. E. Liesegang. *Chemische Fernwirkung. Lieseg. Photograph. Arch.* 1896, 37:305; continued in 37:331, 1896.
2. R. Sultan and A. Abdel-Rahman. On Dynamic Self-Organization: Examples from Magmatic and Other Geochemical Systems. *Latin American Journal of Solids and Structures (LAJSS)* 10:59-73, 2013.
3. Samar Sadek and Rabih Sultan. Liesegang Patterns in Nature: A Diverse Scenery Across the Sciences, a review paper. In: Lagzi I. (ed) *Precipitation Patterns in Reaction-Diffusion Systems*. Research Signpost publications, Trivandrum, Chapter 1, pp. 1-43. 2011.
4. J. H. Kruhl (ed). *Fractals and Dynamic Systems in Geoscience*, Springer-Verlag, Berlin, 1994.
5. R. A. Schibeci and C. Carlsen. An Interseting Student Chemistry Project: Investigating Liesegang Rings. *J. Chem. Educ.* 65:365-366, 1988.
6. H. K. Henisch. *Crystals in Gels and Liesegang Rings*, Cambridge University Press, Cambridge, 1988.
7. R. Sultan and S. Sadek. Patterning Trends and Chaotic Behavior in  $\text{Co}^{2+}/\text{NH}_4\text{OH}$  Liesegang Systems. *J. Phys. Chem.* 100:16912-16920, 1996.
8. Wi. Ostwald, *Lehrbuch der Allgemeinen Chemie*, 2. Aufl., Band II, 2. Teil: Verwandtschaftslehre, Engelmann, Leipzig, 1899, p.779.
9. T. Antal, M. Droz, J. Magnin, Z. Rácz and M. Zrinyi. Derivation of the Matalon-Packter law for Liesegang patterns. *J. Chem. Phys.* 109:9479-9486, 1998.
10. Ferenc Izsák and István Lagzi , A New Universal Law for the Liesegang Pattern Formation. *J. Chem. Phys.* 122:184707-184713, 2005.

11. C. K. Jablczyński. La formation Rythmique des Précipités: Les Anneaux de Liesegang. *Bull. Soc. Chim. Fr.* 33:1592, 1923.
12. N. Kanniah, F. D. Gnanam and P. Ramasamy. *Proc. Indian Acad. Sci., Chem. Sci.* 93:801-811, 1984.
13. T. Karam, H. El-Rassy and R. Sultan. Mechanism of Revert Spacing in a  $\text{PbCrO}_4$  Liesegang System. *J. Phys. Chem. A*, 115:2994-2998, 2011.
14. V. Nasreddine and R. Sultan. Propagating Fronts and Chaotic Dynamics in  $\text{Co}(\text{OH})_2$  Liesegang Systems. *J. Phys. Chem. A* 103:2934-2940, 1999.
15. R. Sultan. Propagating Fronts in Periodic Precipitation Systems with Redissolution. *Phys. Chem. Chem. Phys. (PCCP)* 4:1253-1261, 2002.
16. M. Zrínyi, L. Gálfı́, É. Smidróczi, Z. Rác and F. Horkay. Direct Observation of a Crossover from Heterogeneous Traveling Wave to Liesegang Pattern Formation. *J. Phys. Chem.* 95:1618-1620, 1991.
17. I. Das, A. Pushkarna and N. R. Argawal. Chemical Waves and Light-Induced Spatial Bifurcation in the Mercuric Chloride-Potassium Iodide System in Gel Media. *J. Phys. Chem.* 93:7269-7275, 1989.
18. R. Feeney, P. Ortoleva, P. Strickholm, S. Schmidt and J. Chadam. Periodic Precipitation and Coarsening Waves: Applications of the Competitive Particle Growth Model. *J. Chem. Phys.* 78:1293-1311, 1983.
19. D. S. Chernavskii, A. A. Polezhaev and S. C. Müller. A Model of Pattern Formation by Precipitation. *Physica D* 54, 160-170, 1991.
20. R. Sultan, N. Al-Kassem, A. Sultan and N. Salem. Periodic Trends in Precipitate Patterning Schemes Involving Two Salts. *Phys. Chem. Chem. Phys. (PCCP)* 2, 3155-3162, 2000.
21. P. Ortoleva. *Geochemical Self-Organization*, Oxford University Press, New York, 1994.
22. M. Msharrafieh, M. Al-Ghoul and R. Sultan. Simulation of Geochemical Banding in Acidization-Precipitation Experiments In-Situ. In: M. M. Novak (ed) *Complexus Mundi: Emergent Patterns in Nature*. World Scientific, Singapore, pp. 225-236, 2006.
23. F. Zaknoun, H. El-Rassy, M. Al-Ghoul, S. Al-Joubaily, Th. Mokalled and R. Sultan. Simulation of Geochemical Self-Organization: Acid Infiltration and Mineral Deposition in a Porous Ferruginous Limestone Rock. In: C. H. Skiadas and I. Dimotikalis (eds) *Chaotic Systems: Theory and Applications*. World Scientific, pp. 385-394, 2010.
24. C. Rodríguez-Navarro, O. Cazalia, K. Elert and E. Sebastian. Liesegang Pattern Development in Carbonating Traditional Lime Mortars. *Proc. R. Soc. Lond. A* 458:2261-2273, 2002.
25. M. Matsushita, M. Sano, Y. Hayakawa, H. Honjo and Y. Sawada. Fractal Structures of Zinc Metal Leaves Grown by Electrodeposition. *Phys. Rev. Lett.* 53:286-289, 1984.
26. R. Saab and R. Sultan. Density, Fractal Angle and Fractal Dimension in Linear Zn Electrodeposition Morphology. *J. Non-Equilib. Thermodyn.* 30:321-336, 2005.
27. E. Nakouzi and R. Sultan. Fractal Structures in Two-Metal Electrodeposition Systems I: Pb and Zn. *Chaos* 21:043133, 2011.

28. E. Nakouzi and R. Sultan. Fractal Structures in Two-Metal Electrodeposition Systems II: Cu and Zn. *Chaos* 22:023122, 2012.
29. C. M. Cronemberger and L. C. Sampaio. Growth of Fractal Electrochemical Aggregates Under electric and Magnetic Fields Using a Modified Diffusion-Limited Aggregation Algorithm *Phys. Rev. E* 73:041403, 2006.
30. I. Mogi, M. Kamiko and S. Okubo. Magnetic Field Effects on Fractal Morphology in Electrochemical Deposition. *Physica B* 211:319-322, 1995.
31. Y. Tanimoto, A. Katsuki, H. Yano and Sh. Watanabe. Effect of High Magnetic Field on the Silver Deposition from its Aqueous Solution. *J. Phys. Chem. A* 101:7359-7363, 1997.